Available online at www.sciencedirect.com
SCIENCE DIRECT
Journal of Catalysis 237 (2006) 197–206
JOURNAL OF CATALYSIS
www.elsevier.com/locate/jcat

Au–Ag alloy nanoparticle as catalyst for CO oxidation: Effect of Si/Al ratio of mesoporous support

Aiqin Wang [a], Ya-Ping Hsieh [b], Yong-Fan Chen [b,c], Chung-Yuan Mou [a,c,*]

[a] *Department of Chemistry, National Taiwan University, Taipei, Taiwan 106*
[b] *Department of Physics, National Taiwan University, Taipei, Taiwan 106*
[c] *Center for Condensed Matter Sciences, National Taiwan University, Taipei, Taiwan 106*

Received 18 May 2005; revised 28 October 2005; accepted 31 October 2005

Abstract

Au–Ag alloy nanoparticles deposited on mesoporous support have been found to be catalytically active for CO oxidation. Besides the alloy chemical compositions, the Si/Al ratios of the mesoporous support have a remarkable effect on catalytic activity. The activity for CO oxidation increased with increasing Al content in the support, with the highest catalytic activity obtained when the Si/Al ratio of the support was 24. A series of catalysts with different Si/Al ratio were characterized by XRD, TEM, PL, NMR, and EPR techniques. Both XRD and TEM show that the lower Si/Al ratio leads to the formation of smaller nanoparticles. Photoluminescence (PL) measurement shows that the PL intensity of mesoporous support increased with the Al content, indicating the incorporation of Al promoted the generation of defects in the support. The structure defects produced in the Al-containing mesoporous support play two important roles, in (1) stabilizing alloy nanoparticles and preventing them from sintering during the high temperature treatment and (2) generating the reactive superoxide species, O_2^-, on adsorption of oxygen. EPR measurements show that O_2^- radical intensity on the catalyst surface has a close relation to the Si/Al ratio of the support, and increases with the Al content of the support. A comparison of the O_2^- radicals on the support and on the Au–Ag alloy catalyst reveals that O_2^- radical originates both from the defects on the support and from the Au–Ag nanoparticles. When Au–Ag nanoparticles were deposited onto the support, O_2^- intensity was enhanced greatly. The increase of the catalytic activity with decreasing Si/Al ratio of the support is essentially due to increasing defect sites associated with Al cations. Such defect sites can not only stabilize the alloy nanoparticles, but also favor the activation of O_2 to form reactive O_2^-, leading to an enhanced activity for CO oxidation.

Keywords: Gold; Silver; CO oxidation; Alloy; Mesoporous; Aluminosilicate; Defect; EPR

1. Introduction

Recently, the catalytic properties of gold nanoparticles deposited on metal oxides have attracted much attention since the seminal work of Haruta et al. [1–3]. The gold catalyst system has been proven effective in many oxidation reactions, especially for low-temperature CO oxidation. Four major factors influence the catalytic activity for CO oxidation: the size of gold nanoparticles [4–7], preparation methods [2,5,8–11], pretreatment conditions [12–16], and choice of the support [2,5, 17–19]. Lopez et al. [20] have ordered the different effects into a hierarchy of contributions according to the stabilization ability for reaction intermediates.

With regard to the contribution of supports, most research work has focused on comparison between “active” (often reducible) and “inert” supports [21–24]. However, to date, there is no unambiguous conclusion that whether support participates directly in the catalytic process. Haruta et al. [3] suggested that active supports affect the reactivity by generating the perimeter interfaces around the Au particles as the special catalytic sites. Using DFT calculations, Molina et al. [25] further showed that various Au–MgO interface boundaries have different reactivity for producing suitable Au–Au coordination and for stabilizing reaction intermediate. Their calculation supports Haruta’s findings. In fact, many experiments show that modification of the

* Corresponding author. Fax: +886 2 2366 0954.
E-mail address: cymou@ntu.edu.tw (C.-Y. Mou).

0021-9517/$ – see front matter
doi:10.1016/j.jcat.2005.10.030

support surface structure or morphology can result in enhancement of catalytic activity for CO oxidation [26–30].

Among the highly dispersed Au catalyst systems, Au supported on acidic supports are much less explored because of the lack of a suitable preparation method for them. However, they are potentially important for CO removal in PROX system [3,31]. Acidic supports would be more stable than basic supports because of their minor interaction with the product CO_2. Recently, Okumura et al. [32] observed that gold nanoparticles deposited onto acidic supports such as SiO_2–Al_2O_3 and activated carbon by a gas-phase grafting method had a very low activity for CO oxidation. A highly active Au catalyst on an acidic support for CO oxidation was unknown until recently [33].

Ordered mesoporous aluminosilicate is considered a good catalyst support with well-defined pore size and large surface area. Very small gold particles can be confined into the nanochannels of the silane-functionalized mesoporous silica [34–36]. However, poor catalytic activity was found on such catalysts due to the unremoved organic ligands blocking the active sites [37]. In previous work, we prepared gold nanoparticles of ∼3 nm by functionalization and calcination and found good activity for CO oxidation on Au/MCM-41 [38]. In another approach, we developed a one-pot process to directly embed the Au nanoparticles into the matrices of MCM-41 during its synthesis, and found the catalytic activity to be good [39]. To further improve the catalytic activity of Au/MCM-41, we recently prepared Au–Ag alloy nanoparticles on MCM-41 support by this one-pot synthesis process [40] and found that the catalytic activity is exceptionally high, comparable to the most active catalysts, such as Au/TiO_2 and Au/Fe_2O_3. In this alloy catalyst system, we found some unique properties that are quite different from those of traditional gold catalysts. For example, particle size no longer plays a key role in determining catalytic activity, whereas the composition of the Au/Ag ratio becomes very important [41]. However, such a highly active alloy catalyst is supported on acidic aluminosilicate, traditionally considered "inert." How the support affects the alloy particle size and catalytic activity is not yet clear. In this paper we report in detail the effect of the Si/Al ratio of the support on the catalytic properties of Au–Ag alloy particles, giving special attention to the role of support defects associated with Al incorporation in oxygen activation.

2. Experimental

2.1. Preparation of catalysts

To synthesize the gold–silver alloy nanoparticles supported on mesoporous aluminosilicate in one pot, the first step is to prepare the alloy Au–Ag nanoparticles in aqueous solution. A proper amount of $HAuCl_4$ (Aldrich) and $AgNO_3$ (Acros) was added into an aqueous solution of quaternary ammonium surfactant C_{16}TMAB (Acros) to form a clear yellow solution. Then $NaBH_4$ solution was added dropwise, and a dark-red solution was formed. After that, the Au–Ag alloy nanoparticles solution was poured directly into a sodium aluminosilicate solution with pH value adjusted to about 9.0, after which a red-colored precipitate formed immediately. The gel solution was then transferred to an autoclave to undergo a hydrothermal reaction at 100 °C for 6 h. In all of the sample preparations, the Au/Ag ratio (nominal value) was fixed to 3/1, and the total metal loading was 8 wt%. To get the required Si/Al ratio of the support, the molar ratio in the aluminosilicate gel is 1.0 SiO_2:(0–0.071) $NaAlO_2$:0.18 C_{16}TMAB:493 H_2O. After filtration, washing, drying, and calcination at 560 °C in air, catalysts with differing Si/Al ratios were obtained. The total metal loading and the Si/Al ratio were analyzed by EDX and found to be close to the nominal values within the detection error. The notation of AuAg-MASx in Table 1 means gold–silver nanoparticles supported on mesoporous aluminosilicates, with the Si/Al ratio denoted by x.

Table 1
Textural properties of catalysts with different Si/Al of the support

Sample	Si/Al (mol)	S_{BET} (m^2/g)	V_{pore} (cm^3/g)	Pore size (nm)	FWHM (nm)	Particle size (nm)	
						TEM	XRD
AuAg-MS	∞	752	2.11	2.39	0.306	52.0	26.4
AuAg-MAS74	74	772	2.24	2.22	0.344	37.9	23.4
AuAg-MAS37	37	845	1.70	2.36	0.375	33.7	21.5
AuAg-MAS24	24	834	1.95	2.31	0.388	24.1	17.0
AuAg-MAS14	14	824	1.94	2.09	0.563	14.0	15.1

2.2. Characterization

Room-temperature photoluminescence (PL) was recorded using a SPEX Flurolog-2 instrument equipped with a double-emission monochromator and a R928 photomultiplier tube. Excitation was provided by a 450-W Xe lamp with output focused onto a 0.22-m monochromator to provide wavelength selection.

Transmission electron microscopy (TEM) images of the catalysts were obtained using a JEOL JEM-2010 transmission electron microscope with an operating voltage of 200 kV. Samples were dispersed in ethanol, and a drop of the obtained suspension was fixed on a microgrid covered with amorphous carbon film.

The powder X-ray diffraction (XRD) patterns were collected on a PANalytical X′Pert PRO instrument operating at a 45 kV and a current of 40 mA with Cu-K_α radiation in the 2θ range from 1.5° to 10° and from 20° to 80°. Nitrogen adsorption-desorption isotherms were obtained at 77 K on a Micromeritics ASAP 2010 apparatus, and the pore size distribution was calculated from the nitrogen adsorption isotherm using the BJH (Barrett–Joyner–Halenda) method.

^{27}Al NMR was recorded with Bruker MLS-500 NMR spectrometer at a frequency of 104.22 MHz, spinning rate of 8 kHz, pulse length of 1.0 μs, delay time of 0.2 s, and spectra width of 330 ppm. The ^{27}Al chemical shifts are reported in relation to the solution of aluminum nitrate.

Electron paramagnetic resonance (EPR) spectra were recorded at 84 K with a Bruker EMX spectrometer working in the X-band (9.53 GHz). Before measurement, the catalysts were first reduced at 600 °C with 10% H_2/N_2, then exposed to air. Then weighted catalyst of 20 mg was placed inside a 4-mm-o.d. quartz tube with greaseless stopcocks, and then evacuated

at room temperature until the residual pressure was below 1×10^{-3} Torr.

2.3. Activity measurements

CO oxidation reaction was performed in a continuous-flow fixed-bed microreactor. Each experiment used 0.04 g of catalyst. Before measurement, the catalyst was prereduced in situ in 10% H_2 in N_2 at 600 °C for 1 h. The reactant gases were purified by 4 Å molecular sieves, then mixed and flowed into the reactor for the reaction. Thus, the water vapor content in the reactant stream was no more than 4 ppm. The reactant flow consisted of a mixture of 1% CO and 4% O_2 with He as balance. A total gas flow of 66.7 mL min^{-1} was applied corresponding to a GHSV of about 100,000 mL g_{cat}^{-1} h^{-1}. The reaction temperature was controlled within ±1 °C by a thermocouple in contact with the inlet of the catalyst bed. The reactants and products were analyzed on-line with a HP6890 gas chromatograph equipped with a Carboxen 1000 column and thermal conductivity detector. The CO conversion is defined as the amount of CO_2 produced divided by the total amount of CO fed to the catalyst. The conversion data were reproducible within 5% accuracy.

3. Results

3.1. Textural properties of catalysts with different Si/Al ratio

Fig. 1 shows a typical low-angle XRD pattern and N_2 adsorption–desorption isotherm of the catalyst with a Si/Al ratio of 24. There is only one peak at $2\theta = 1.986°$ in the low-angle range, and no higher-order Bragg reflection peaks were observed, indicating a worm-like and disordered mesostructure. From the nitrogen adsorption–desorption isotherm (Fig. 1), one can see that besides the mesopores characteristic of the capillary condensation at $p/p_0 \sim 0.35$–0.40, there is an extraordinarily large jump of adsorption at p/p_0 near 1. This is because that in our preparation procedure, a rapid neutralization step was used to form the nanosized mesoporous particles. The textural macropores formed by the agglomeration of the nanosized MCM-41 particles are thus prominent. The interparticle macropores [42] would facilitate transport of reactant and product molecules during the catalytic reaction, making the Au/MCM more accessible for CO oxidation, and thus allowing the higher CO conversion to be obtained [39].

Table 1 lists the textural properties of catalysts with different Si/Al ratios. From Table 1, one can see that upon varying the Si/Al ratio, the BET surface areas of the catalysts are 700–800 m^2/g and the pore sizes are 2.0–2.4 nm. The pore volume of the support material is relatively large compared with traditional MCM-41 material, because of textural porosity. On the other hand, the full width at half maximum of the pore size distribution increases with increasing Al content, indicating that the pore structure became more disordered with Al content of the supports. In fact, for the sample with Si/Al = 14, we cannot observe any XRD peaks in the low-angle range, indicating a very disordered structure.

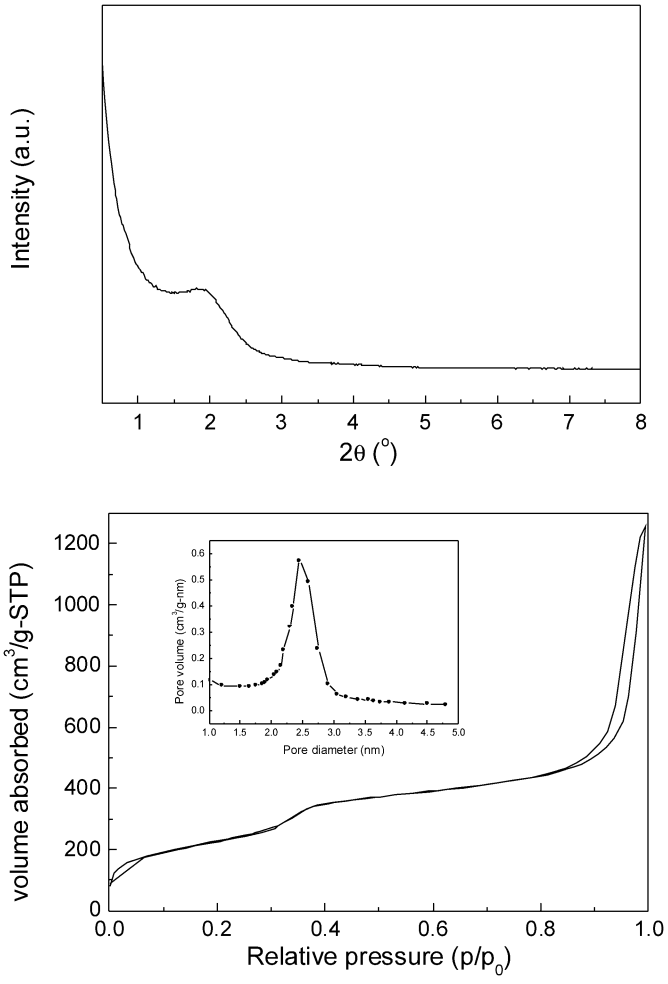

Fig. 1. (top) Low-angle XRD pattern of AuAg-MAS24. (bottom) N_2 adsorption–desorption isotherm and pore size distribution (inset) of AuAg-MAS24.

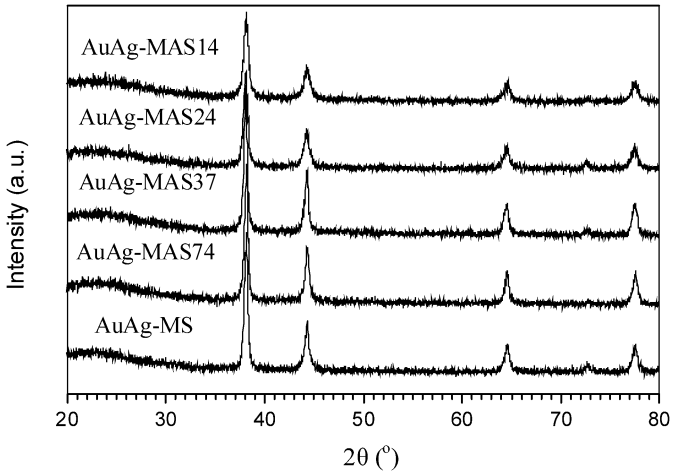

Fig. 2. Wide-angle XRD patterns of catalysts with different support Si/Al ratios.

3.2. Wide-angle XRD patterns

Fig. 2 shows the wide-angle XRD patterns of catalysts with different Si/Al ratios. The four peaks positioned at $2\theta = 38.2°$, 44.3°, 64.5°, and 77.6° correspond to the (111), (200), (220),

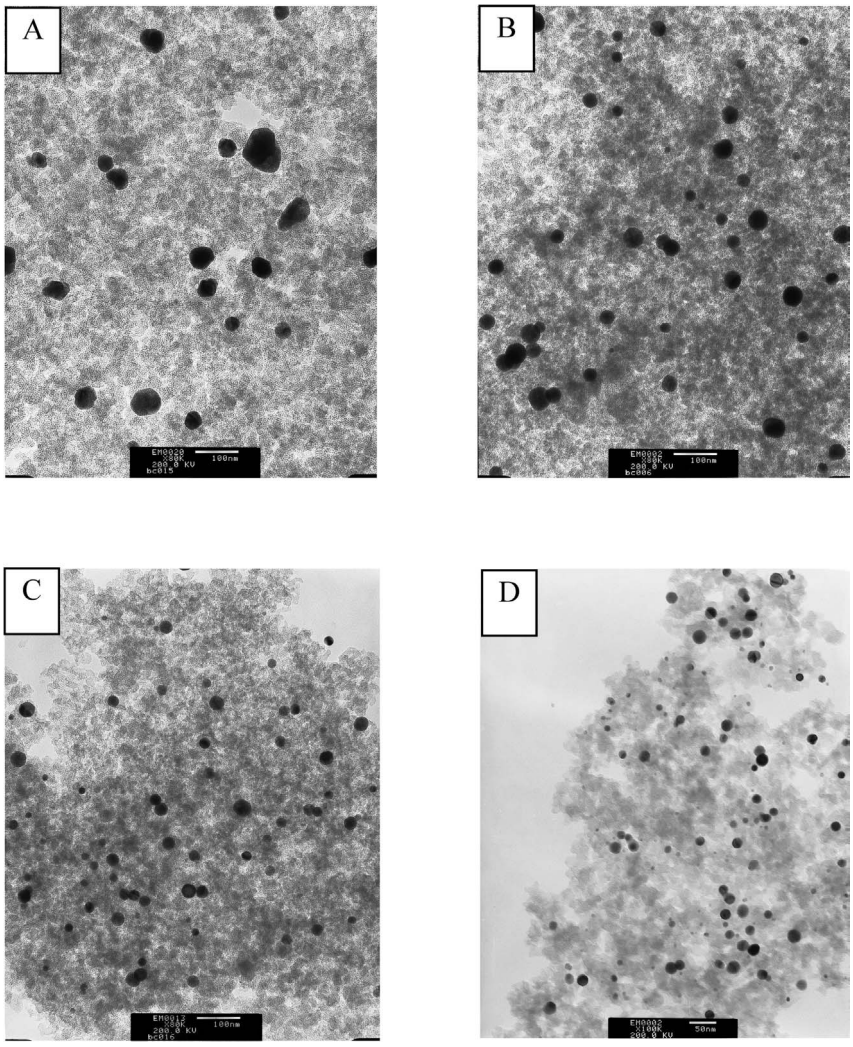

Fig. 3. TEM images of catalysts with different support Si/Al ratios (A) ∞, (B) 37, (C) 24, (D) 14. The scale bar in (A), (B) and (C) is 100 nm, in (D) – 50 nm.

and (311) lattice planes of the Au, Ag, or Au–Ag alloys. Because Au and Ag have the same fcc structure and almost the same lattice constant, we can not distinguish gold–silver alloy from a mixture of the monometallic phases from just the XRD patterns [43]. However, in our previous work [41], we confirmed from EXAFS and UV–vis studies that nanoparticles of Au–Ag alloy were formed after reduction pretreatment. The four XRD peaks presented here should be due to alloys of Au–Ag. One can see that the XRD peaks become broader with increasing Al content in the samples. An estimate of particle sizes from the peak width of the (111) reflection using Scherrer's equation [44] is given in Table 1. It is clear that the particle size of the Au–Ag alloy becomes smaller with increasing Al content of the support. This result is confirmed by TEM observations.

3.3. TEM characterization of catalysts

Figs. 3 and 4 show the TEM images and the corresponding particle size distributions of the four catalysts with Si/Al ratios of ∞, 37, 24, and 14, respectively. One can see that on the three Al-containing mesoporous support (MAS), the Au–Ag alloy particles are mostly spherical, and the average particle size decreases with increasing Al content (33.7, 24.1, and 14.0 nm for the three samples). Especially for the sample with the highest Al content (Si/Al ratio of 14), nanoparticles <5 nm in size were observed. In contrast, on the pure siliceous mesoporous support, particle shape was irregular and average particle size increased to about 52 nm, in good agreement with the XRD results. Clearly, the Al-containing mesoporous support can better stabilize the metal nanoparticles deposited on it to limit their sizes. We suspect that this may be related to the structural defects induced by incorporation of Al into the framework. PL measurements are thus performed to clarify the relationship between structural defects and the Al content of the support.

3.4. Photoluminescence spectra

PL measurement can provide useful information about the structural defects of aluminosilicates. For mesoporous MCM-41 material, various types of defects, such as nonbridging oxygen hole centers, twofold-coordinated silicon centers, and other oxygen-related defects, have been found to be responsible for the origin of PL [45–51]. Fig. 5 shows the PL spectra of the

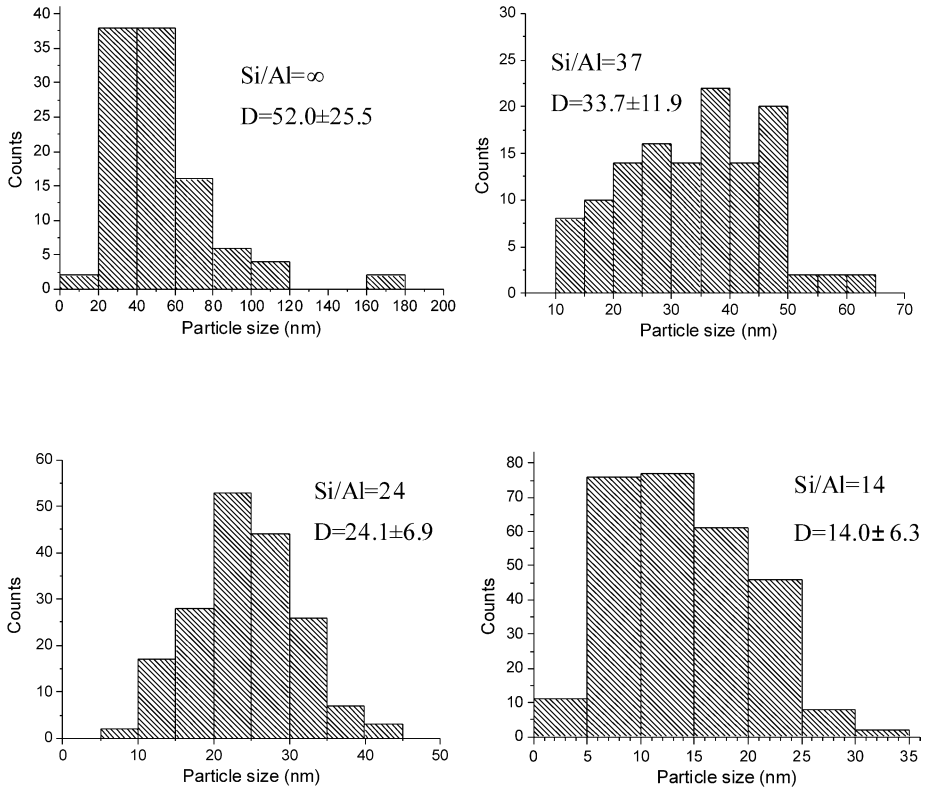

Fig. 4. Size histogram of AuAg particles deposited on mesoporous support with different Si/Al ratios.

MCM-41 support with various Si/Al ratios measured under excitation by a 270-nm light. All of the supports had a broad blue emission band in the range of 300–500 nm. Moreover, PL intensity increased significantly with increasing Al content. Compared with pure siliceous MCM-41 (MS in Fig. 5), there was an enhancement of about two orders of intensity for the Al-containing MAS samples. Gaussian fitting [51] of the PL spectra of Al-containing samples (e.g., MAS24, as shown in Fig. 5B) revealed three emission bands with peaks at ∼350, ∼390, and ∼428 nm. The two bands at ∼350 and ∼428 nm were also observed in the pure siliceous MS sample, as shown in the inset of Fig. 5A. According to literature and our PL excitation measurements, the band at ∼350 nm was due to some oxygen excess defects such as Si–O–O–Si in MCM-41 [49], and the band at ∼428 nm originated from triplet-to-singlet transition in twofold-coordinated silicon centers [46–48]. These two types of structural defects are often observed in silica materials. On the other hand, the emission band at ∼390 nm was not observed in pure siliceous MCM-41. Clearly, it is associated with incorporation of Al into the MCM-41 framework. The PL band at ∼390 nm is often observed on alumina material and is assigned to the F^+ centers (oxygen vacancy with one electron) [50,51]. Accordingly, we assign the emission band at ∼390 nm in Al-containing MCM-41 supports to the F^+ centers, which were generated by the incorporation of Al into the framework of MCM-41. The density of F^+ centers increased with the Al content; therefore, the major effect of aluminum incorporation in MCM-41 is the generation of rich defects, accompanied by the loss of structural order.

When Au–Ag alloy particles were deposited onto Al-MCM-41 support, the PL intensity decreased dramatically, becoming even lower than the original pure siliceous MCM-41, as shown in Fig. 5A. The quenching of the PL by alloy nanoparticles is probably due to an excited electron transfer to the nearby metals.

3.5. *UV–vis spectra of the catalysts*

Au–Ag alloy is known to have distinct surface plasmon resonances (SPRs) [52–54]. The absorption bands are influenced mainly by the surface chemical compositions (Au/Ag ratio). Fig. 6 shows the UV–vis spectra of the catalysts with differing Si/Al ratios of the support. All of the catalysts have the same SPR band positioned at ∼473 nm, suggesting that the surface chemical compositions of the catalysts are almost the same, no matter what the Si/Al ratio of the support. This is important when we study the support effect of different catalysts, because the effect of changing surface Au/Ag ratio is precluded.

3.6. *^{27}Al MAS NMR spectra*

To reveal the coordinate environment of Al in the support, ^{27}Al MAS NMR spectra were recorded (Fig. 7). All of the Al-containing catalysts show two NMR peaks. The strong peak positioned at around 53 ppm is attributed to the presence of aluminum in tetrahedral coordination, indicating that most of the Al species in the support are in tetrahedral coordination. The weak peak at around 0 ppm is ascribed to the extra-framework

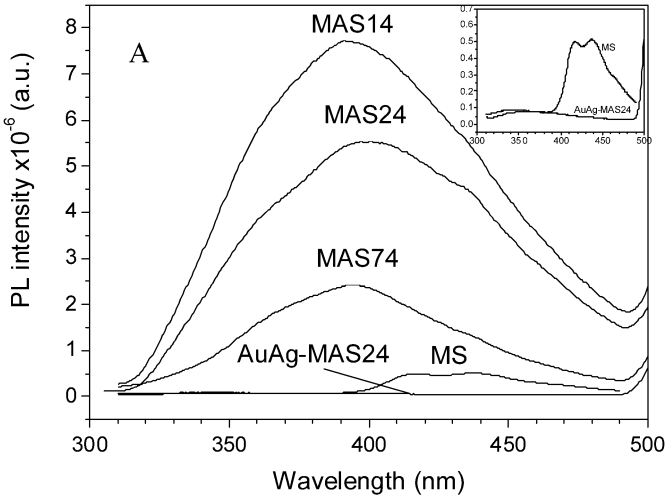

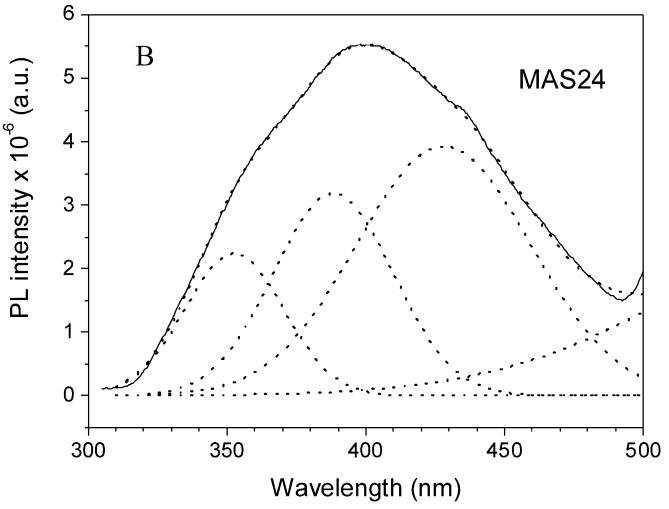

Fig. 5. (A) Photoluminescence spectra of MCM-41 and AuAg-MAS with different Si/Al ratios. The inset is the PL spectra of MS and AuAg-MAS24. (B) Gaussian fitting of PL of MAS24.

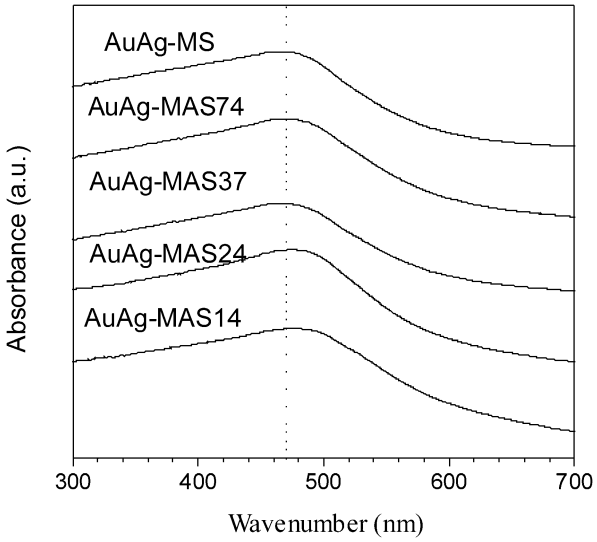

Fig. 6. UV–vis absorption spectra of catalysts.

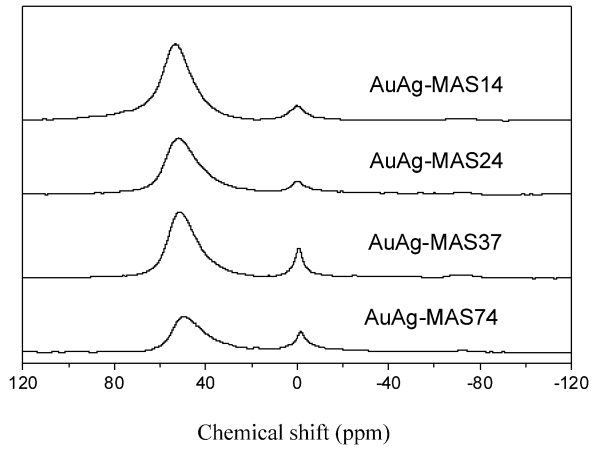

Fig. 7. ^{27}Al MAS NMR of catalysts with different Si/Al ratios.

octahedral aluminum species. This may arise from framework dealumination during the calcination process [55].

3.7. EPR spectra

To determine the contribution of support to the CO oxidation, EPR spectra were recorded on the supports and on the Au–Ag alloy catalysts (Figs. 8 and 9). Fig. 8 shows that on the pure siliceous MCM-41 support, no EPR signal was detected at 84 K. However, for the Al-containing supports, a weak EPR signal appeared at $g = 2.010$. Moreover, the intensity of this signal increased with increasing Al content.

Fig. 9 shows the EPR spectra of the Au–Ag alloy catalysts with different Si/Al ratios in the support. There is only one signal at $g = 2.009$, and the signal intensity increased with increasing Al content. In addition, compared with the EPR signals of the support in Fig. 8, the shape and position of the peaks in two cases are almost the same, suggesting that they originate

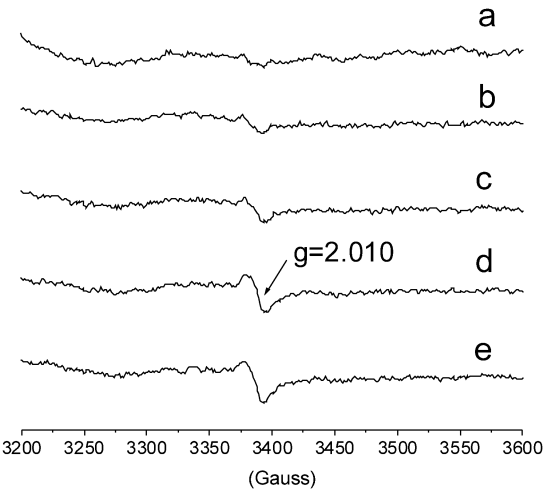

Fig. 8. EPR spectra of mesoporous supports with different Si/Al ratios. (a) Si/Al = ∞; (b) Si/Al = 74; (c) Si/Al = 37; (d) Si/Al = 24; (e) Si/Al = 14.

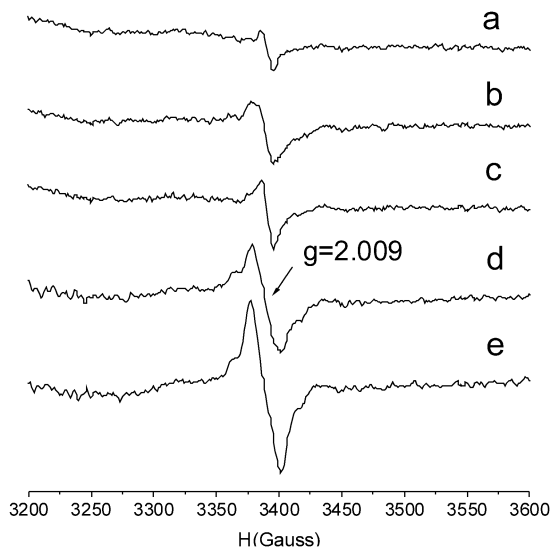

Fig. 9. EPR spectra of catalysts with different Si/Al ratios. (a) Si/Al = ∞; (b) Si/Al = 74; (c) Si/Al = 37; (d) Si/Al = 24; (e) Si/Al = 14.

from the same species. Moreover, when Au–Ag nanoparticles were deposited onto the support, the intensity of EPR signals increased markedly. An EPR signal was observed even for the AuAg-MS, which does not contain Al in the support. These findings imply that the observed EPR signals arise from contributions of both the support and the Au–Ag nanoparticles.

3.8. Activity of the catalysts with different Si/Al ratio

Fig. 10 depicts the catalytic performance of samples with different Si/Al ratios. From Fig. 10A, one can see that CO can be converted at room temperature over all of the catalysts with or without Al in the support, but the catalysts containing Al in the support are much more active than the catalysts without Al in the support. With an Si/Al ratio of 24 or 37, CO can be completely converted at room temperature. In contrast, when the support did not contain Al, CO conversion was <90%. Moreover, we note that within 4 h of time on stream, the CO conversion over AuAg-MS decreased gradually, while the CO conversion over AuAg-MAS24 remained at 100%, suggesting that AuAg-MAS24 is more active and stable than AuAg-MS. In fact, in a previous paper [41] we investigated the stability of AuAg-MAS24 and found that the CO conversion decreased from 100% only to 95% after a 100-h run on the reaction stream.

Compared with the dramatic effect on catalytic activity from changing the Au/Ag ratio [40,41], the effect of changing the Al content of the support is indeed weaker. To better distinguish the effect of Al content, we studied the temperature dependence of these catalysts. Fig. 10B shows that on all of the catalysts investigated, CO oxidation occurred at temperatures as low as −17 °C. The CO conversions at −17 °C follow an order according to the Si/Al ratio in the support: Si/Al (24) > Si/Al (14) > Si/Al (37) > Si/Al (74) > Si/Al (∞). The temperature dependence of the conversion profiles indicates that all of the investigated catalysts show an activity valley when the temperature rises from 80 to 160 °C, which is characteristic of the Au–Ag bimetallic catalyst system [40,41].

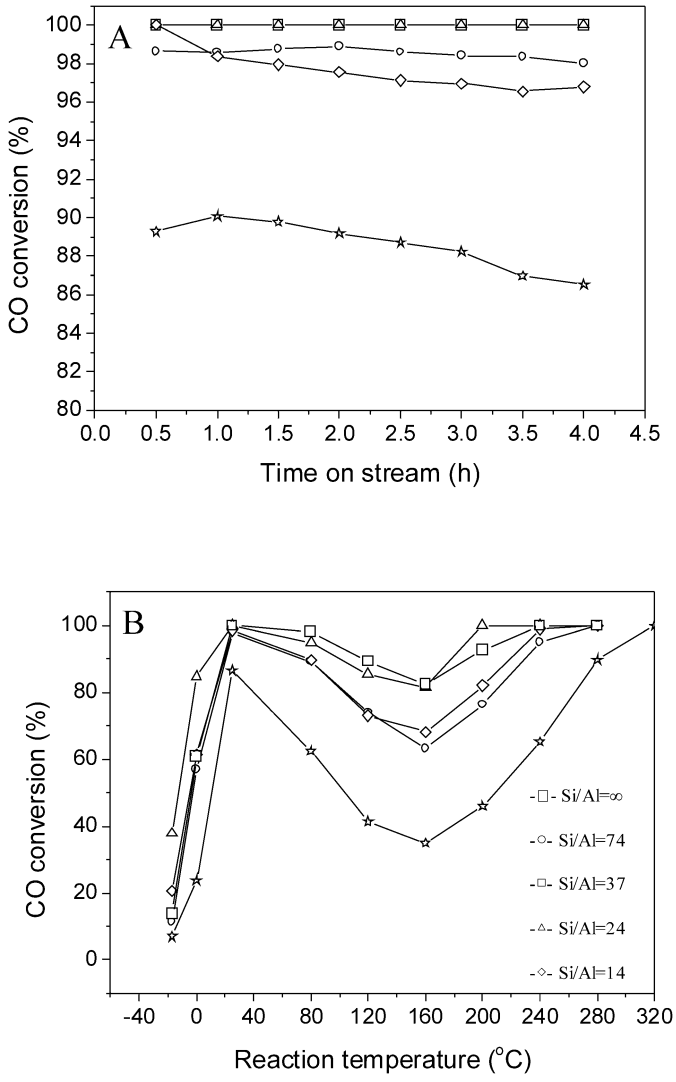

Fig. 10. (A) CO conversions with time on stream at room temperature. (B) CO conversion profiles versus reaction temperature over 5 catalyst samples: (☆) AuAg-MS; (○) AuAg-MAS74; (□) AuAg-MAS37; (△) AuAg-MAS24; (◇) AuAg-MAS14.

Table 2
Comparison of activity for CO oxidation on different catalysts

Catalyst	Temperature (°C)	Reaction rate ($mol_{CO}\ g_{Au}^{-1}\ s^{-1}$)	TOF_{TEM} (s^{-1})	References
AuAg-MS	−17	1.09×10^{-6}	0.089	This work
AuAg-MAS74	−17	1.78×10^{-6}	0.106	This work
AuAg-MAS37	−17	2.11×10^{-6}	0.113	This work
AuAg-MAS24	−17	5.89×10^{-6}	0.700	This work
AuAg-MAS14	−17	3.19×10^{-6}	0.071	This work
Au/Fe_2O_3	0	–	0.138	[2]
Au/TiO_2	0	–	0.124	[2]
Au/Co_3O_4	0	–	0.175	[2]

Table 2 lists the reaction rate and turnover frequencies (TOFs) at −17 °C for CO oxidation over catalysts with varying Al content in the support. The TOFs were calculated on the basis of number of surface alloy atoms, which were estimated

from mean alloy particle sizes assuming a spherical shape of the alloy particles according to the TEM images. TOF clearly increases with increasing Al content, attaining the highest value of 0.7 s^{-1} with a Si/Al ratio of 24, then decreasing to 0.071 s^{-1} with further increases in Al content to a Si/Al ratio of 14. Moreover, compared with the most active catalysts reported in the literature [2], such as Au/TiO_2, Au/Fe_2O_3 and Au/Co_3O_4, our AuAg-MAS24 catalyst is more active.

4. Discussion

4.1. Stabilizing effect of Al on the alloy particle size

As discussed earlier (Sections 3.2 and 3.3), we know that the Al content of the support has a great influence on the size distribution of the Au–Ag alloy nanoparticles deposited on it. The Au–Ag particle size decreases significantly with increasing Al content of the support. It should be mentioned that in our preparation procedure, the Au–Ag alloy particles were preformed in aqueous solution before being deposited onto the mesoporous support. The preformed colloidal Au–Ag nanoparticles are <10 nm in size [40]. However, after being deposited onto the mesoporous aluminosilicate support and then calcined at high temperatures, particle size grows and varies with the Si/Al ratio of the support. To clarify how the incorporation of Al stabilized the alloy particles, we must first know the reason for particle sintering. As shown by the XRD patterns in Fig. 11, after being deposited onto the mesoporous support and subjected to hydrothermal treatment, particle size remains essentially unchanged (∼5 nm, as estimated from Scherrer's equation). Therefore, at this stage, the Au–Ag alloy particles do not interact with the support, and the difference in the Si/Al ratio of the support does not cause the change in alloy particle size. However, during the calcination process to remove the surfactant, the particle size enlarges greatly due to sintering. The higher the Al content of the support, the smaller the alloy particle size. This trend strongly suggests that nanoparticle mobility becomes sluggish due to the incorporation of Al. A detailed study on the structural changes during calcination and reduction with EXAFS [56] reveals that complete phase segregation occurred during the calcination process, leading to the formation of AgBr phase and metallic Au phase. The formation of AgBr largely accelerates particle sintering during high-temperature calcination. Because the incorporation of Al into mesoporous framework creates rich defects, especially the F^+ centers, as shown by our PL results, we believe that these defects act as anchoring sites to make the nanoparticles less mobile during the calcination process. Probably the F^+ center, which has one electron, can interact strongly with the AgBr enriched on the particle surface, thus decreasing particle mobility. After subsequent reduction with H_2 at high temperatures, Br^- species were completely removed, and the Au–Ag alloy was reformed. This reduction treatment at high temperature is the key step in activating the catalyst, although the particle size remained unchanged at this stage. Therefore, the support defects created by Al incorporation are favorable for obtaining smaller particles. Using DFT calculations, Lopez et al. [57] found that the final

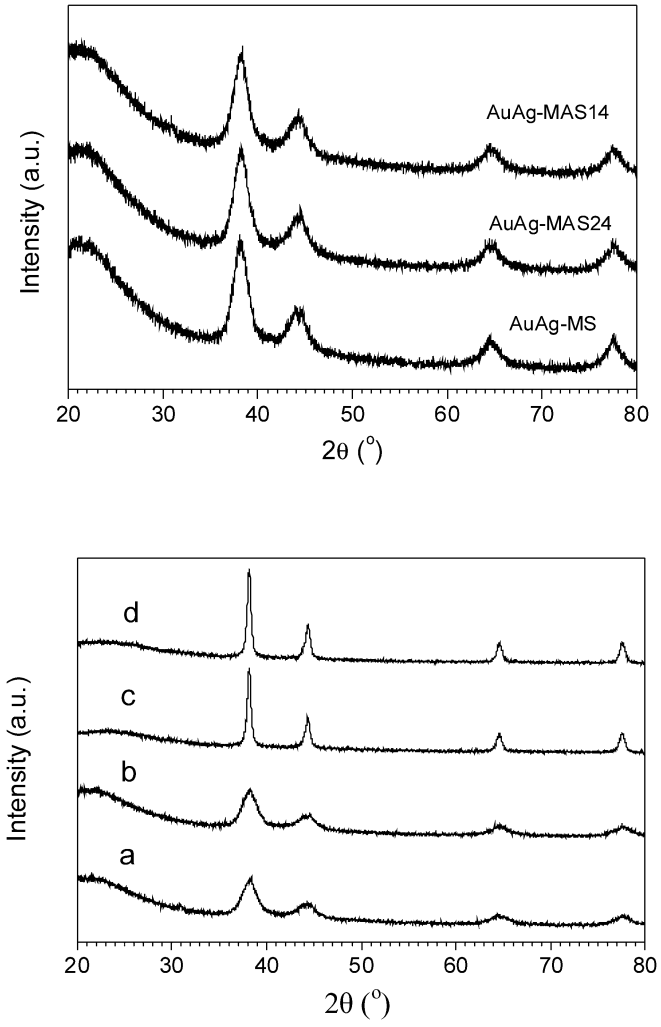

Fig. 11. (top) Wide-angle XRD patterns of as-synthesized samples with different Al content in the support. (bottom) Wide-angle XRD patterns of AuAg-MAS24 (a) as-synthesized; (b) after hydrothermal treatment at 100 °C for 6 h; (c) after calcined at 560 °C for 6 h; (d) after reduction at 600 °C for 1 h.

size and shape of the gold particles is determined by the support defects. For example, their calculations show that gold particles do not bind to a perfect TiO_2 surface, but have a binding energy of about 1.6 eV defect on an oxygen vacancy in TiO_2. Their conclusion supports our findings.

4.2. Activation of O_2 promoted by Al incorporation

Many experiments and theoretical calculations show that the adsorption and activation of O_2 is the key step in CO oxidation. Thus, the activity of catalytic oxidation of CO is determined mainly by the activation of oxygen to the superoxide species. The subsequent oxygen transfer to the CO molecule adsorbed on the neighboring Au sites is fast. EPR is a sensitive technique for detecting spin species in the catalyst. Li and Vannice [58] studied Ag nanoparticles on SiO_2 using EPR and found a single sharp symmetric signal at $g = 2.0028 \pm 0.0002$ for all of the investigated Ag/SiO_2 samples with different Ag particle sizes, which they ascribed to the conducting electron (CESR) only for small Ag nanoparticles (<7 nm). However, Claus et al. [59] in-

vestigated the EPR spectra of Au/TiO_2 and observed a narrow singlet at $g = 2.0053$ on reduced Au/TiO_2, which they ascribed not to the CESR of nanosized Au particles, but rather to paramagnetic defects of the support. Similarly, Okumura et al. [60] studied the interaction between CO and O_2 on Au/TiO_2 and Au/Al_2O_3 using EPR; after O_2 adsorption, a signal appeared at $g = 2.009$ which was ascribed to the O_2^- radicals stabilized on surface Ti^{4+} species. For Au/Al_2O_3, these authors observed a similar EPR signal at $g = 2.010$, which was also ascribed to the O_2^- radicals stabilized on Al cations.

For our samples, CESR can be excluded in consideration of our peak position (not at $g = 2.002$) and the fact that the particle sizes of our bimetallic nanoparticles are probably too large to give CESR. According to the position of the EPR signals that we have observed, we assign the EPR signals at $g = 2.009 \pm 0.001$ to O_2^-. The PL spectra verify the existence of rich defects (F^+ centers) on the Al-containing supports. It is known that F^+ centers can act as sites for O_2 adsorption by transferring one electron to the adsorbed O_2, to form the superoxide species O_2^- on the defect sites. Therefore, the EPR signals that we have observed on the mesoporous aluminosilicate support probably originate from the O_2^- stabilized on defects associated with Al cations. The observations that there is no EPR signal on pure siliceous support and that EPR signal intensity increases with increasing Al content confirm our assignment, and this is also consistent with our PL results.

Deposition of Au–Ag nanoparticles onto the aluminosilicate support significantly increased the intensity of the EPR signals. Kondarides and Verykios [43] found that the molecular oxygen adsorption on Ag is favored by the presence of Au. In a previous paper [41] we showed that molecular oxygen can be easily adsorbed on Au–Ag alloy to form O_2^-. Therefore, the higher EPR signals on the alloy catalysts compared with those on the support may be due to the combination of O_2^- formed on the support itself and also formed on the Au–Ag nanoparticles. Thus, the incorporation of Al into the mesoporous framework can promote the adsorption of oxygen on the catalyst surface.

4.3. Promotion effect of Al on the catalytic activity

In Section 3.8 we noted that activity (TOF) increased with increasing Al content in the support in all of the Au–Ag alloy catalysts except AuAg-MAS14. Our EPR results show that O_2^- concentration on the catalyst surface is proportional to the Al content of the support, whereas TEM shows that alloy particle size decreases with Al content. Thus one of the causes of Al promotion in CO oxidation is the formation of smaller metallic particles and thus greater adsorption of oxygen on higher surface areas. But this surface area effect is only part of the reason, because TOF data show a significant enhancement of TOF at $Si/Al = 24$. We propose that the F^+ centers created by Al incorporation can facilitate the adsorption of oxygen, as confirmed by EPR. If the Au–Ag alloy particles are near the F^+ centers, then the activated oxygen on the defects can spill over to the nearby Au–Ag alloy particles to react with the activated CO on Au sites, leading to enhanced activity. However, in this case, long-distance spillover of O_2^- species from F^+ centers to CO–Au sites must occur. On the other hand, as shown in Fig. 9, active O_2^- species are produced in much greater quantities at Ag sites of the Au–Ag particles. In this case, spillover of O_2^- species is not necessary, because O_2^-–Ag and CO–Au exist in the nearest neighbor. The two different pathways of oxygen activation explain why the Al-promoting effect is minor compared with the Ag-promoting effect. Nonetheless, it must be pointed out that too high an Al content in the support will destroy the ordering of pore structure, which is confirmed by the disappearance of XRD peaks in the low-angle range with a decrease in Si/Al ratio from 24 to 14. This may explain the decreased catalytic activity of AuAg-MAS14. Recently, we have observed the similar trend of catalytic activity of gold particles with Al content in the mesoporous support SBA-15 [33]. However, it should be mentioned that the decrease in Si/Al leads not only to increased defect concentration, but also to increased –OH concentration on the support. The role of –OH (or acidity) in the enhancement of activity is not clear yet. The role of Al merits further study.

5. Conclusion

In summary, we have studied the catalyst system of gold–silver alloy nanoparticles deposited on mesoporous aluminosilicate support. Our findings indicate that the Si/Al ratio of the support has an important effect on the catalytic activity of CO oxidation. We observed an increase in superoxide species O_2^- with increasing Al content. Also, TEM analyses showed a decrease in particle size of Au–Ag alloy with increasing Al-content. These two factors lead to the increase in activity with increasing of Al content. However, excessive incorporation of Al into the mesoporous framework causes some loss of structure order, leading to decreased catalytic activity with a Si/Al ratio of 14.

We then investigated the origin of increased superoxide production with increased Al content in the support. EPR and PL studies indicated that the incorporation of Al promoted the generation of rich defects on the support. Such defects as those associated with tetrahedral Al not only stabilize the Au–Ag alloy nanoparticles and thus prevent them from sintering, but also promote the activation of oxygen by electron transfer to adsorbed oxygen to form superoxide. The superoxide species then react with adsorbed (on Au sites) CO to form carbon dioxide. Because we have shown that our gold–silver nanocatalyst system is very active in oxygen activation, either by Ag or by the defects on the aluminosilicate support, it will be highly interesting to investigate whether this AuAg alloy catalyst may be applied to other oxidation reactions, or if the superoxide species can also be observed in other oxidation reactions, such as in hydrogen peroxide production [61].

Acknowledgments

This work was supported by the National Science Council of Taiwan. Discussions on EPR measurements with Professor Tom Lin are acknowledged.

References

[1] M. Haruta, T. Kobayashi, H. Sano, N. Yamada, Chem. Lett. (1987) 405.
[2] M. Haruta, Catal. Today 36 (1997) 153.
[3] M. Haruta, Chem. Record 3 (2003) 75.
[4] M. Valden, X. Lai, D.W. Goodman, Science 281 (1998) 1647.
[5] G.C. Bond, D. Thompson, Catal. Rev. Sci. Eng. 41 (1999) 319.
[6] W.T. Wallace, R.L. Whetten, J. Phys. Chem. B 104 (2000) 10964.
[7] D.C. Meier, D.W. Goodman, J. Am. Chem. Soc. 126 (2004) 1892.
[8] H. Liu, A.I. Kozlov, A.P. Kozlova, T. Shido, K. Asakura, Y. Iwasawa, J. Catal. 185 (1999) 252.
[9] A.I. Kozlov, A.P. Kozlova, K. Asakura, Y. Matsui, T. Kogure, T. Shido, Y. Iwasawa, J. Catal. 196 (2000) 56.
[10] Y.J. Chen, C.T. Yeh, J. Catal. 200 (2001) 59.
[11] F. Moreau, G.C. Bond, A.O. Taylor, Chem. Commun. (2004) 1642.
[12] F. Boccuzzi, A. Chiorino, M. Manzoli, Ping Lu, T. Akita, S. Ichikawa, M. Haruta, J. Catal. 202 (2001) 256.
[13] C.H. Lin, S.D. Lin, J.F. Lee, Catal. Lett. 89 (2003) 235.
[14] C.K. Costello, J. Guzman, J.H. Yang, Y.M. Wang, M.C. Kung, B.C. Gates, H.H. Kung, J. Phys. Chem. B 108 (2004) 12529.
[15] Z.P. Qu, M.J. Cheng, X.L. Dong, X.H. Bao, Catal. Today 93–95 (2004) 247.
[16] Y. Iizuka, A. Kawamoto, K. Akita, M. Daté, S. Tsubota, M. Okumura, M. Haruta, Catal. Lett. 97 (2004) 203.
[17] W.S. Epling, G.B. Hoflund, J.F. Weaver, J. Phys. Chem. 100 (1996) 9929.
[18] A. Baiker, M. Maciejewski, S. Tagliaferri, P. Hug, J. Catal. 151 (1995) 407.
[19] R.J.H. Grisel, B.E. Nieuwenhuys, J. Catal. 199 (2001) 48.
[20] N. Lopez, T.V.W. Janssens, B.S. Clausen, Y. Xu, M. Mavrikakis, T. Bligaard, J.K. Norskov, J. Catal. 223 (2004) 232.
[21] J.D. Grunwaldt, M. Maciejewski, O.S. Becker, P. Fabrizioli, A. Baiker, J. Catal. 186 (1999) 458.
[22] M.M. Schubert, S. Hackenberg, A.C. van Veen, M. Muhler, V. Plzak, R.J. Behm, J. Catal. 197 (2001) 113.
[23] S.H. Overbury, L. Ortiz-Soto, H. Zhu, B. Lee, M.D. Amiridis, S. Dai, Catal. Lett. 95 (2004) 99.
[24] S. Arrii, F. Morfin, A.J. Renouprez, J.L. Rousset, J. Am. Chem. Soc. 126 (2004) 1199.
[25] L.M. Molina, B. Hammer, Phys. Rev. B 69 (2004) 155424.
[26] A.P. Kozlova, S. Sugiyama, A.I. Kozlov, K. Asakura, Y. Iwasawa, J. Catal. 176 (1998) 426.
[27] W. Yan, B. Chen, S.M. Mahurin, E.W. Hagaman, S. Dai, S.H. Overbury, J. Phys. Chem. B 108 (2004) 2793.
[28] W. Yan, B. Chen, S.M. Mahurin, S. Dai, S.H. Overbury, Chem. Commun. (2004) 1918.
[29] W. Yan, B. Chen, S.M. Mahurin, V. Schwartz, D.R. Mullins, A.R. Lupini, S.J. Pennycook, S. Dai, S.H. Overbury, J. Phys. Chem. B 109 (2005) 10676.
[30] S. Carrettin, P. Concepcion, A. Corma, J.M. Lopez Nieto, V.F. Puntes, Angew. Chem. Int. Ed. 43 (2004) 2538.
[31] D. Cameron, R. Holliday, D. Thompson, J. Power Sources 118 (2003) 298.
[32] M. Okumura, S. Tsubota, M. Haruta, J. Mol. Catal. A 199 (2003) 73.
[33] C.W. Chiang, A.Q. Wang, B.Z. Wan, C.Y. Mou, J. Phys. Chem. B 109 (2005) 18042.
[34] Z. Kónya, V.F. Puntes, I. Kiricsi, J. Zhu, J.W. Ager, M.K. Ko, H. Frei, P. Alivisatos, G.A. Somorjai, Chem. Mater. 15 (2003) 1242.
[35] C.M. Yang, P.H. Liu, Y.F. Ho, C.Y. Chiu, K.J. Chao, Chem. Mater. 15 (2003) 275.
[36] B. Lee, H. Zhu, Z. Zhang, S.H. Overbury, S. Dai, Microporous Mesoporous Mater. 70 (2004) 71.
[37] C.M. Yang, M. Kalwei, F. Schüth, K.J. Chao, Appl. Catal. A 254 (2003) 289.
[38] Y.S. Chi, H.P. Lin, C.Y. Mou, Appl. Catal. A 284 (2005) 199.
[39] (a) H.P. Lin, Y.S. Chi, J.N. Lin, C.Y. Mou, B.Z. Wan, Chem. Lett. (2001) 1116;
(b) J.H. Liu, Y.S. Chi, H.P. Lin, C.Y. Mou, B.Z. Wan, Catal. Today 93–95 (2004) 141.
[40] J.H. Liu, A.Q. Wang, Y.S. Chi, H.P. Lin, C.Y. Mou, J. Phys. Chem. B 109 (2005) 40.
[41] A.Q. Wang, J.H. Liu, S.D. Lin, T.S. Lin, C.Y. Mou, J. Catal. 233 (2005) 186.
[42] M.C. Chao, H.P. Lin, C.Y. Mou, Chem. Lett. 33 (2004) 672.
[43] D.I. Kondarides, X.E. Verykios, J. Catal. 158 (1996) 363.
[44] J. Luo, M.M. Maye, V. Petkov, N.N. Kariuki, L. Wang, P. Njoki, D. Mott, Y. Lin, C.J. Zhong, Chem. Mater. 17 (2005) 3086.
[45] S. Dzwigaj, J.M. Krafft, M. Che, S. Lim, G.L. Haller, J. Phys. Chem. B 107 (2003) 3856.
[46] M.E. Gimon-Kinsel, K. Groothuis, K.J. Balkus Jr., Microporous Mesoporous Mater. 20 (1998) 67.
[47] N. He, S. Ge, C. Yang, C. Hu, M. Gu, Mater. Res. Bull. 39 (2004) 1931.
[48] J.L. Shen, C.F. Cheng, Curr. Opin. Solid State Mater. Sci. 7 (2003) 427.
[49] G.G. Qin, J. Lin, J.Q. Duan, G.Q. Yao, Appl. Phys. Lett. 69 (1996) 1689.
[50] X.S. Peng, L.D. Zhang, G.W. Meng, X.F. Wang, Y.W. Wang, C.Z. Wang, G.S. Wu, J. Phys. Chem. B 106 (2002) 11163.
[51] W.L. Xu, M.J. Zheng, S. Wu, W.Z. Shen, Appl. Phys. Lett. 85 (2004) 4364.
[52] M.P. Mallin, C.J. Murphy, Nano Lett. 2 (2002) 1235.
[53] I. Lee, S.W. Han, K. Kim, Chem. Commun. (2001) 1782.
[54] S. Link, Z.L. Wang, M.A. EI-Sayed, J. Phys. Chem. B 103 (1999) 3529.
[55] S. Udayakumar, A. Pandurangan, P.K. Sinha, Appl. Catal. A 272 (2004) 267.
[56] A.Q. Wang, C.M. Chang, C.Y. Mou, J. Phys. Chem. B 109 (2005) 18860.
[57] N. Lopez, J.K. Nørskov, T.V.W. Janssens, A. Carlsson, A. Puig-Molina, B.S. Clausen, J.D. Grunwaldt, J. Catal. 225 (2004) 86.
[58] X.M. Li, A. Vannice, J. Catal. 151 (1995) 87.
[59] P. Claus, A. Brückner, C. Mohr, H. Hofmeister, J. Am. Chem. Soc. 122 (2000) 11430.
[60] M. Okumura, J.M. Coronado, J. Soria, M. Haruta, J.C. Conesa, J. Catal. 203 (2001) 168.
[61] C. Sivadinarayana, T.V. Choudhary, L.L. Daemen, J. Eckert, D.W. Goodman, J. Am. Chem. Soc. 126 (2004) 38.